The Journal of Veterinary Medical Science

NOTE

Surgery

Repeated surgical treatment and long-term outcome of a cat with vertebral vascular hamartoma

Daisuke ITO[1)]*, Naoko SHIOZAWA[1)], Naoki SEKIGUCHI[1)], Chieko ISHIKAWA[1)], Nick D. JEFFERY[2)] and Masato KITAGAWA[1)]

[1)]School of Veterinary Medicine, Nihon University, Kameino 1866, Fujisawa, Kanagawa 252-0880, Japan
[2)]Department of Small Animal Clinical Sciences, Texas A&M University, TX77843, USA

J. Vet. Med. Sci.
82(6): 721–725, 2020
doi: 10.1292/jvms.19-0079

Received: 5 February 2019
Accepted: 27 March 2020
Advanced Epub:
16 April 2020

ABSTRACT. A 30-month-old Maine Coon presented with progressive proprioceptive ataxia, paraparesis, thoracolumbar pain, and decreased appetite. An extradural mass was detected within the left side of the 13th thoracic vertebral canal that compressed the spinal cord on magnetic resonance (MR) and was considered to be mineralized on computed tomography (CT) images. The resected mass was diagnosed as a vertebral vascular hamartoma. Clinical signs improved, but recurrence was diagnosed by MR and CT imaging at 7 months after surgery. Repeated excisional surgery yielded the same diagnosis and the clinical signs abated. Fifteen months after the second surgery, there was apparent vertebral deformation, but there was no further change on CT images by 29 months.

KEY WORDS: feline, magnetic resonance imaging, paraparesis, spinal cord tumor

A 30-month-old neutered male Maine Coon cat weighing 4.5 kg presented to the Animal Medical Center at Nihon University with progressive proprioceptive pelvic limb ataxia, paraparesis, thoracolumbar pain, and decreased appetite. The clinical signs had been observed 4 weeks before referral, and the cat's neurological function had gradually deteriorated since then. Initially, treatment with robenacoxib (2 mg/kg, administered subcutaneously) at the referring veterinary hospital was associated with improved appetite and reduction in thoracolumbar pain, but the pelvic limb ataxia and paresis continued to worsen, resulting in nonambulatory paraparesis. At this stage, robenacoxib was replaced with prednisone at 0.5 mg/kg per day (per orem), and the cat's neurological condition slightly improved. When referred, the cat showed ambulatory paresis and proprioceptive ataxia in the pelvic limbs and repeatable evidence of thoracolumbar hyperesthesia on palpation. Neurological examination detected decreased postural reactions and exaggerated spinal reflexes in the pelvic limbs. No cranial nerve or thoracic limb deficits were apparent, indicating a neuroanatomical localization within the T3–L3 spinal cord segments. Physical examination revealed no enlargement of superficial lymph nodes. Hematological and serum biochemistry values were within normal ranges.

Based on the findings of thoracolumbar and abdominal radiographies and ultrasound exploration of the abdominal organs and lymph nodes, unremarkable results were observed. The cat was anesthetized and underwent magnetic resonance imaging (MRI) of the thoracolumbar region in ventral recumbency using a 1.5 Tesla scanner (EXCELART Vantage, Canon Medical Systems Corp., Tochigi, Japan). T1-weighted (Repetition Time: TR 450–500 msec, Echo Time: TE 15 msec), T2-weighted (TR 4,000 msec, TE 120 msec), and fluid-attenuated inversion recovery (FLAIR) (TR 8,000 msec, TE 108 msec) images were obtained in transverse and sagittal orientation with slice thickness of 3 mm and 2 mm, respectively, and 0.5-mm interspaces. Contrast T1-weighted images were obtained after the intravenous injection of a contrast medium (0.2 m*l*/kg, ProHance, Eisai, Tokyo, Japan). On the left side of the vertebral canal within T13 vertebra, there was a solitary focal mass that deviated the spinal cord toward the right (Fig. 1A–C). The mass was more iso- to hypointense on T1-weighted images (Fig. 1A, 1D), mostly hyperintense and partially hypointense in its ventral part on T2-weighted images (Fig. 1B), and more mixed iso- and hyperintense on FLAIR images compared with the normal spinal cord parenchyma. At the interface between the spinal cord and the lesion at its cranial and caudal limits on sagittal images, there was a distinct line that was hyperintense on T1- and T2-weigted images (Fig. 1D). The mass was strongly and homogenously hyperintense on contrast-enhanced (CE) T1-weighted images (Fig. 1C, 1E). In addition to the mass lesion, the vertebral body of T13 was more hypointense on T1-weighted and more hyperintense on T2-weighted images compared with the adjacent vertebral bodies (T12 and L1) and was strongly enhanced on CE T1-weighted images (Fig. 1E).

Computed tomography (CT) images of the thoracolumbar vertebrae were obtained using a 16-slice helical scanner (Aquilion

*Correspondence to: Ito, D.: itou.daisuke@nihon-u.ac.jp

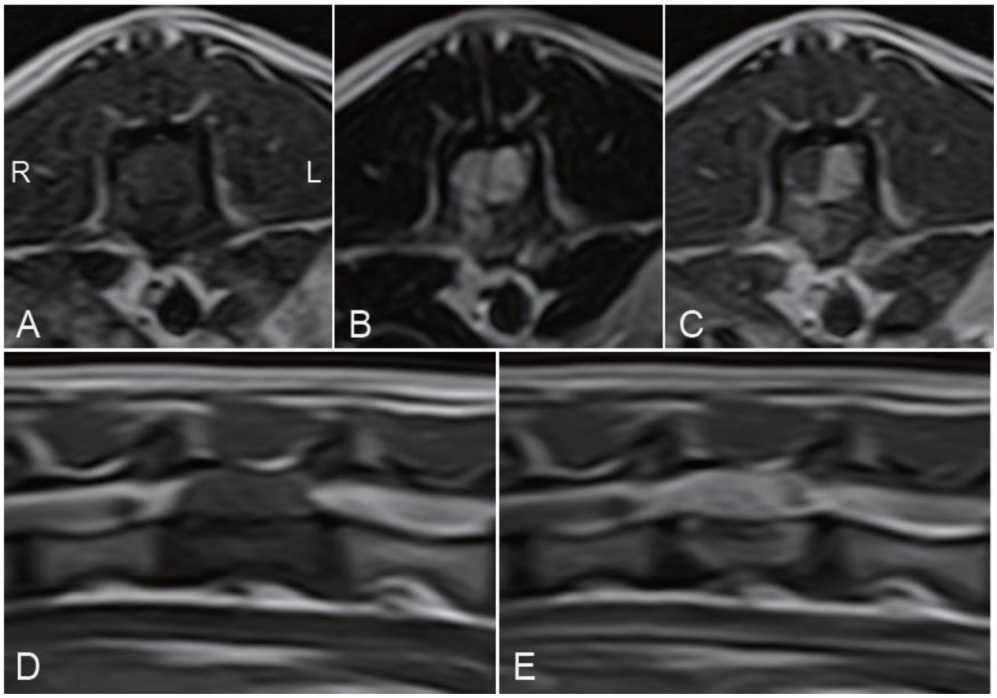

Fig. 1. Transverse T1-weighted (A), T2-weighted (B), and post-contrast T1-weighted images (C) through the mid-body of T13 and midline sagittal T1-weighted (D) and post-contrast T1-weighted images (E) at initial presentation. There is a focal mass lesion in the left vertebral canal of T13 causing spinal cord displacement (A–C). Most of the mass is more homogenously iso- to hypointense on T1-weighted images (A, D) and more hyperintense on T2-weighted images (B) compared with the spinal cord parenchyma. There is marked homogenous enhancement of the mass (C, E) and T13 vertebral body (E).

16, Canon Medical Systems Corp.) under the following conditions: 120 kVp, 200 mA, and 1.0-mm slice thickness. The previously identified mass had an attenuation density consistent with mineralization (pre-contrast mean 396 Hounsfield Unit: HU, post-contrast mean 781 HU) (Fig. 2A). The left pedicle and lamina were not affected where the mass was attached, but periosteal reaction and hyperostosis were suspected in the left ventral side of T13 vertebral body.

Analyses of cerebrospinal fluid, obtained by lumbar (L5–L6) puncture, and urine including cell population, pH level, and concentrations of protein and glucose were within reference intervals, and bacterial culture was negative. Because there was no history of previous trauma and no evidence of infection, the most likely differential diagnoses were considered to be neoplastic (e.g., osteosarcoma, osteoma, hemangioma, lymphoma and peripheral nerve sheath tumor) or malformation (e.g., vertebral vascular hamartoma) based on the imaging characteristics and clinical presentation.

Although some periosteal reaction and hyperostosis were suspected in the ventral part of the vertebral body, left pediculectomy, which minimizes possible induced instability of the vertebrae, was performed to resect the mass lesion using a surgical microscope. Grossly, the outer cortical bone of the vertebral arch was normal, but microscopically the cancellous bone was thickened with a porous structure that comprised several thin layers of cortical-like bone and hemorrhagic soft tissues between the layers that resembled trabecular bone. The mass lesion also comprised hemorrhagic tissues and thin layers of cortical-like bone (Fig. 3). Moderate hemorrhage was observed while drilling the bone and excising the mass. The pediculectomy was continued until normal cortical and cancellous bone were apparent. Subsequently, CT images were obtained to confirm that the mass was completely excised (Fig. 2B).

Resected tissues were submitted for histopathological examination and bacterial culture. Sections of samples fixed with 10% formalin were stained with hematoxylin and eosin. Small caliber blood vessels formed by proliferating endothelial cells were surrounded by a loose myxoid stroma and mineralized struts of trabecular bone (Fig. 4). Histologically, all components of the structures were differentiated into normal tissue types, and no inflammatory response or anaplastic cells were observed. The histopathological diagnosis was vertebral vascular hamartoma. There was no evidence of infection on cultured specimens.

At 3-week recheck after surgery, neurological dysfunction in the pelvic limbs and thoracolumbar pain had regressed. At 7 months after surgery, there was recurrence of ambulatory paraparesis without thoracolumbar pain, and neurological examination suggested a neuroanatomical localization at the same site as the initial presentation. Because thoracolumbar radiographs were inconclusive, MRI and CT of the thoracolumbar region were repeated (from this period, CT images were obtained using a 320-slice helical scanner [Aquilion ONE, Canon Medical Systems Corp.] under the following conditions: 120 kVp, maximum 350 mA, and 0.5-mm slice thickness). On MRI, a solitary focal mass was recognized in the left vertebral canal of the T13 where the original mass had been. The mass was more hypointense in its ventral part and isointense in the dorsal portion on T1-weighted images and

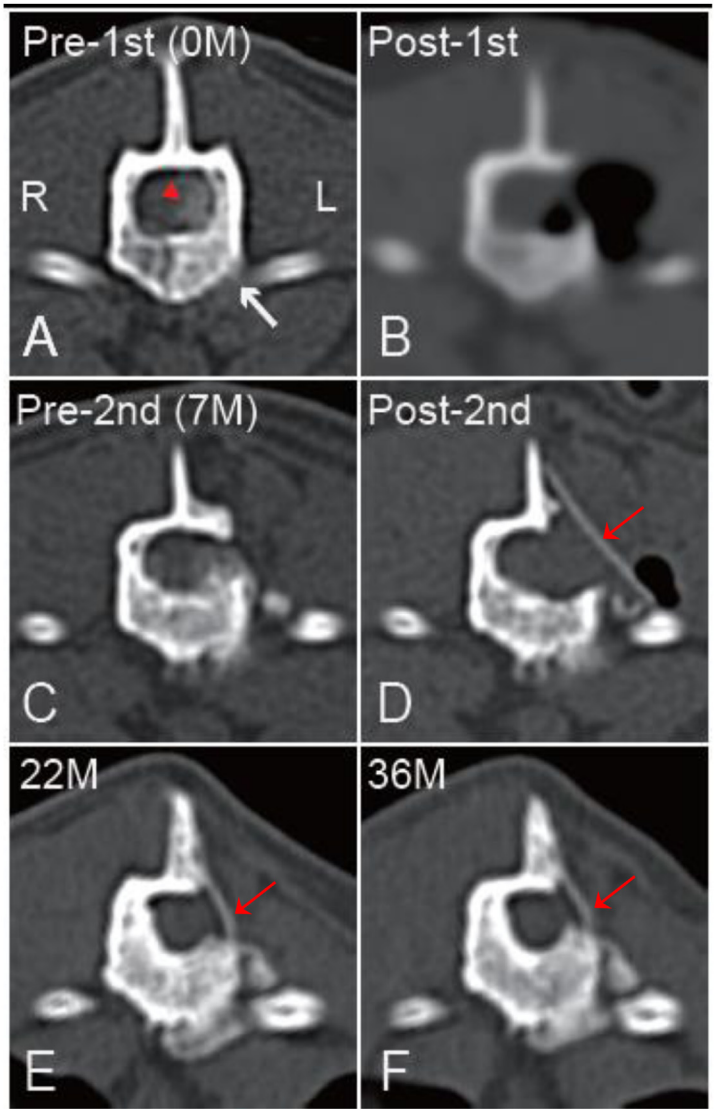

Fig. 2. Transverse computed tomography (CT) images through the mid-body of T13 at initial CT scan (A), immediately after the first surgery (B), 7 months after the first surgery when neurological signs recurred (C), immediately after second surgery (D), 22 months later (15 months after the second surgery) (E), and 36 months later (29 months after the second surgery) (F). A calcified mass in the left vertebral canal and vertebral deformation was detected (A, arrowhead). The mass was resected by surgery (B) but recurred, and vertebra deformation progressed (C). The central canal was narrowed at 15 months after the second surgery due to hypertrophy of the right pedicle (E), but did not change after 29 months from the second surgery (F). The spinous process of the vertebra was hypertrophied at 15 months after the second surgery. (A) and (B) were obtained using a 16-slice helical scanner (Aquilion 16, Canon Medical Systems Corp., Tochigi, Japan) under the following conditions: slice thickness, 1.0 mm; reconstruction interval, 0.5 mm; and scan filter, none. (C)–(F) are obtained using a 320-slice helical scanner (Aquilion ONE, Canon Medical Systems Corp.) with the following conditions: slice thickness, 0.5 mm; reconstruction interval, 0.5 mm; and scan filter, none. Display algorithm: A: FC81 (bone) (window width, 2,000; window level, 500), B (adjusted window width, 2,000; window level, 500 from FC27) (head, soft tissue), C–F: FC30 (bone) (window width, 2,000; window level, 500). Red arrows represent an artificial dura mater (expanded polytetrafluoroethylene surgical membrane) (GORE-TEX, W. L. Gore & Associates, Inc., Santa Clare, CA, USA).

more iso- to hypointense in the ventral portion and hyperintense in its dorsal part on T2-weighted and FLAIR images compared to normal spinal cord parenchyma. The ventral part of the mass was mildly enhanced and the dorsal part strongly enhanced on CE T1-weighted images. On CT images, the dorsal part showed attenuation characteristics of mineralization (pre-contrast mean 134 HU, post-contrast mean 230 HU), and the ventral portion attenuated at a level between mineralization and bone matrix (pre-contrast mean 627 HU, post-contrast mean 633 HU) (Fig. 2C). The left vertebral body was deformed due to periosteal reaction and hyperostosis, and the left vertebral arch (lamina) was thickened due to hyperostosis.

A second surgical procedure, using a combination of hemilaminectomy (extension of the initial pediculectomy) and partial corpectomy, was performed to excise the mass and thickened the vertebral arch (lamina), articular process, and part of the vertebral body under a surgical microscope. After the mass lesion was excised, an artificial dura mater (expanded polytetrafluoroethylene surgical membrane) (GORE-TEX, W. L. Gore & Associates, Inc., Santa Clare, CA, USA) was placed at the site of hemilaminectomy and pediculectomy. Subsequently, CT images were obtained to confirm that the mass had been resected (Fig. 2D). Histopathological findings were the same as those in the initial report.

At 15 months and 29 months after the second surgery, the owner requested repeat CT images to check the lesion, although the cat was neurologically normal (our CT scanner allowed taking images without general anesthesia or sedation). CT images at 15 months after the second surgery revealed that the whole T13 vertebral body, including the right side vertebral arch, articular process, and spinous process, was more thickened compared with CT images taken immediately after the second surgery (Fig. 2D, 2E), but these findings were unchanged at 29 months after the second surgery (Fig. 2F). There was progressive hypertrophy of the left 13th rib over the 22-month period following the initial CT scan, although the right-sided 13th rib was normal (Fig. 5).

To the best of our knowledge, this is the first report describing the follow-up images of vertebral vascular hamartoma in a cat with lesion recurrence. A hamartoma is an overgrowth of a normal organ due to excessive proliferation of various cells of

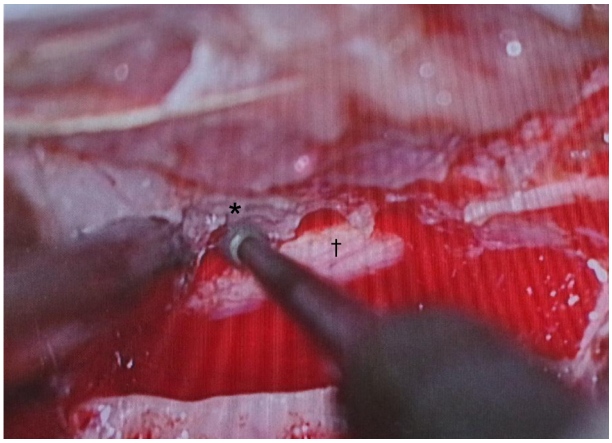

Fig. 3. Gross findings of the mass lesion during decompressive surgery. The mass grossly comprised hemorrhagic soft tissues and thin layers of cortical-like bone (asterisk). During excision, moderate hemorrhage was observed. Dagger: spinal cord.

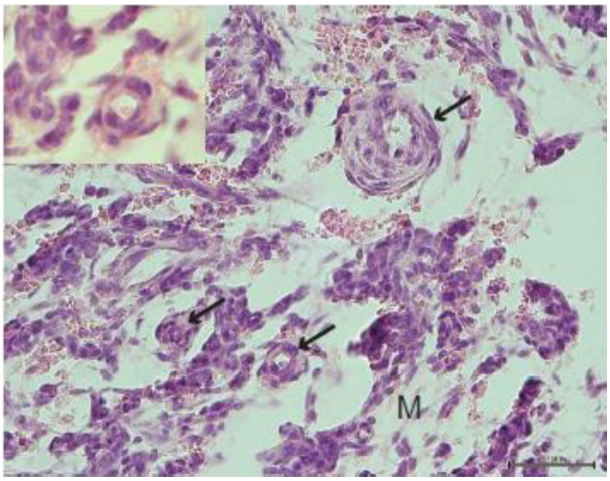

Fig. 4. Hematoxylin and eosin section at 400× magnification showing irregular proliferation of endothelial cells that form numerous small caliber blood vessels (arrows). There is loose myxoid stroma (M) surrounding the vessels. Inset shows endothelial cells at higher magnification (1,000×). Bar represents 50 μm.

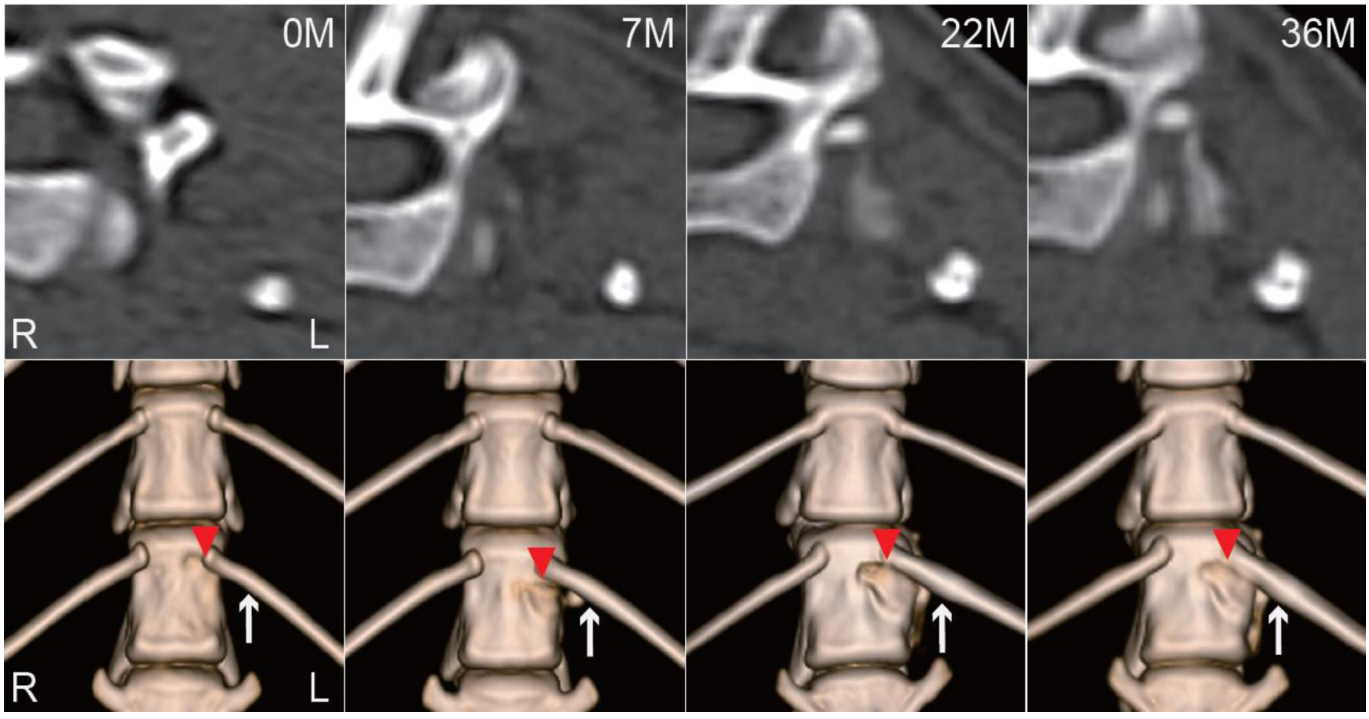

Fig. 5. Serial follow-up multi-planar reconstruction of the left 13th ribs (upper row) and three-dimensional (3D) images of the 13th ribs (lower row, ventral view). The transverse shape of the left rib was changed at 22 months (M) but not changed at 36 months after the initial computed tomography scan. Hypertrophy of the rib and left vertebral body was detected on 3D images after 22 months (arrows) and 7 months, respectively (arrowheads). Display algorithm: FC81 (bone) (window width, 2,000; window level, 500 for image at 0 month) and FC30 (bone) (window width, 2,000; window level, 500 for images at 7, 22, and 36 months).

different tissue types that is usually considered nonneoplastic [4]. In humans, hamartomas are classified as vascular (angiomatous), lipomatous, chondroid, or neurogenic according to the primary tissue type [12]. Although histologically normal, sometimes a hamartoma is defined as a benign tumor because the organ overgrowth can lead to functional impairment of adjacent tissues and recur at the original site [12]. In small animals, hamartomas have been reported in dogs [1, 2, 6, 7, 11] and cats [3, 5, 8–10] in different organs, and vertebral vascular hamartoma has been previously reported in two cats [5, 10].

Vertebral vascular hamartoma was first described in a 15-month-old cat with a cervical lesion showing gait impairment [5]. The cat improved neurologically after surgery and had a good outcome during a 2-year period without follow-up imaging. The second case was a 9-month-old cat that had a lumbar vertebral vascular hamartoma [10]; clinical signs improved after surgical treatment without recurrence at 1-year follow-up examination, although follow-up images were not available. In contrast to the previous two cases, our case showed recurrence of neurological signs at 7 months after the initial surgery associated with recurrence of the hamartoma at the original site. Additionally, follow-up CT images 15 months after second surgery revealed that the whole vertebra became progressively deformed but, surprisingly, did not progress subsequently. Although vascular hamartoma can potentially recur at its site of origin because of its continuous growth pattern [4], this growth is self-limited in mature animals [12]. This behavior of hamartoma would explain why the lesion in our case showed recurrence at relatively short period after surgical resection but subsequently did not recur over the long subsequent follow-up period. In the treatment of human patients with vascular hamartoma, complete surgical resection is recommended to achieve a low risk of recurrence [4]. In our case, initially, we had selected pediculectomy as a minimally invasive approach, but it proved insufficient to adequately resect the affected tissues.

CT findings were similar to those reported previously [5, 10], but the signal intensity of the lesion on MRI was slightly different [10]. In a previous report, the peripheral part of the lesion was more iso- to hyperintense on T2-weighted images and more hypointense on T1-weighted images compared with normal spinal cord parenchyma. In the central part, it was hypointense on T1- and T2-weighted images. Moderate enhancement after the injection of a contrast medium was observed. In contrast, in our case, the lesion was predominantly homogenous and hyperintense on T2-weighted images and hypo- to isointense on T1-weighted images, with strong enhancement after the injection of a contrast medium. Therefore, the signal intensity characteristics of vertebral vascular hamartoma in the cat appear to be variable. In our case, the signal intensity of T13 vertebral body differed from that of the adjacent vertebra and was strongly enhanced on post-contrast T1-weighted images, suggesting that the whole vertebra was affected by vascular hamartoma at the initial presentation.

In conclusion, this case report described the long-term follow-up MRI and CT images and outcome of a cat with a vascular hamartoma arising from the thoracic vertebra. The short-term prognosis after excisional surgery was good, which was similar to the prognoses of previous reports [5, 10], but the long-term clinical outcome included recurrence, which was inconsistent with the long-term clinical outcomes of previous reports. The recurrence suggests that surgical approaches for these lesions might need to be extensive and complete resection might be difficult in some cases.

REFERENCES

1. Chanoit, G., Mathews, K. G., Keene, B. W., Small, M. T. and Linder, K. 2012. Surgical treatment of a pulmonary artery vascular hamartoma in a dog. *J. Am. Vet. Med. Assoc.* **240**: 858–862. [Medline] [CrossRef]
2. Kuhlman, G. M., Taylor, A. R., Thieman-Mankin, K. M., Griffin, J., Cook, A. K. and Levine, J. M. 2016. Use of a frameless computed tomography-guided stereotactic biopsy system for nasal biopsy in five dogs. *J. Am. Vet. Med. Assoc.* **248**: 929–934. [Medline] [CrossRef]
3. Martin-Vaquero, P., Moore, S. A., Wolk, K. E. and Oglesbee, M. J. 2011. Cerebral vascular hamartoma in a geriatric cat. *J. Feline Med. Surg.* **13**: 286–290. [Medline] [CrossRef]
4. Morris, G. F., Murphy, K., Rorke, L. B. and James, H. E. 1998. Spinal hamartomas: a distinct clinical entity. *J. Neurosurg.* **88**: 954–957. [Medline] [CrossRef]
5. Parkes, J. D., Kline, K. L., Riedesel, E. A. and Haynes, J. S. 2009. A vascular hamartoma arising from the cervical spine of a cat. *J. Feline Med. Surg.* **11**: 724–727. [Medline] [CrossRef]
6. Sanders, S. G., Bagley, R. S., Gavin, P. R., Konzik, R. L. and Cantor, G. H. 2002. Surgical treatment of an intramedullary spinal cord hamartoma in a dog. *J. Am. Vet. Med. Assoc.* **221**: 659–661, 643–644. [Medline] [CrossRef]
7. Scott, S. J., Elliot, K., Philibert, H., Summers, B. A., Godson, D., Singh, B. and Simko, E. 2015. An unusual lipomatous brain mass in a Golden Retriever dog. *J. Vet. Diagn. Invest.* **27**: 772–776. [Medline] [CrossRef]
8. Smith, T. J., Baltzer, W. I., Ruaux, C. G., Heidel, J. R. and Carney, P. 2010. Gastric smooth muscle hamartoma in a cat. *J. Feline Med. Surg.* **12**: 334–337. [Medline] [CrossRef]
9. Stalin, C. E., Granger, N. and Jeffery, N. D. 2008. Cerebellar vascular hamartoma in a British Shorthair cat. *J. Feline Med. Surg.* **10**: 206–211. [Medline] [CrossRef]
10. Taylor-Brown, F. E., Lamb, C. R., Martineau, H., Muir, C. and Beltran, E. 2018. Imaging diagnosis- imaging and histopathologic characteristic of a vertebral hamartoma in a cat. *Vet. Radiol. Ultrasound* **59**: E12–E16. [Medline] [CrossRef]
11. Tjostheim, S. S., Kellihan, H. B., Csomos, R. A., McAnulty, J. and Steinberg, H. 2015. Vascular hamartoma in the right ventricle of a dog: Diagnosis and treatment. *J. Vet. Cardiol.* **17**: 321–328. [Medline] [CrossRef]
12. Winters, J. R., Davis, B. L. and Melzer, J. M. 2016. A recurrent, slow-growing retropharyngeal lesion. *JAMA Otolaryngol. Head Neck Surg.* **142**: 599–600. [Medline] [CrossRef]